human tracheal epithelial cells expressing high amounts of terminal α2,6 SA motifs and, simultaneously, in an improved ability to overcome the inhibitory effects of human bronchial mucins associated with α2,3 SA receptors (*28*). However, mutations that caused a shift from the avian-type to human-type receptor binding specificity for the H1 subtype do not cause an equivalent shift in specificity for the H5 subtype (*24*). Likewise, the amino acid changes required to alter the H3 HA from an avian- to human-type receptor binding specificity are different from those required for the H1 HA. Therefore, it is likely that different avian HA subtypes have different structural requirements to confer receptor specificity. Thus, it is currently unknown which additional mutations in the H5 HA would cause a shift to the human-type specificity, which may be required for H5N1 viruses to transmit efficiently among humans.

References and Notes

1. W. H. Frost, *Public Health Rep.* **35**, 584 (1920).
2. F. Burnet, E. Clark, *Influenza: A Survey of the Last 50 Years in the Light of Modern Work on the Virus of Epidemic Influenza* (MacMillan, Melbourne, 1942).
3. T. M. Tumpey *et al.*, *Science* **310**, 77 (2005).
4. J. C. Kash *et al.*, *Nature* **443**, 578 (2006).
5. D. Kobasa *et al.*, *Nature* **431**, 703 (2004).
6. K. D. Patterson, G. F. Pyle, *Bull. Hist. Med.* **65**, 4 (1991).
7. C. Viboud *et al.*, *Vaccine* **24**, 6701 (2006).
8. World Health Organization, "Epidemic and pandemic alert and response (EPR): Avian influenza" (available at www.who.int/csr/disease/avian_influenza/en/index.html).
9. C. B. Bridges *et al.*, *J. Infect. Dis.* **185**, 1005 (2002).
10. J. M. Katz *et al.*, *J. Infect. Dis.* **180**, 1763 (1999).
11. T. R. Maines *et al.*, *Proc. Natl. Acad. Sci. U.S.A.* **103**, 12121 (2006).
12. T. Ito *et al.*, *J. Virol.* **72**, 7367 (1998).
13. M. Matrosovich *et al.*, *J. Virol.* **74**, 8502 (2000).
14. R. J. Connor *et al.*, *Virology* **205**, 17 (1994).
15. L. Glaser *et al.*, *J. Virol.* **79**, 11533 (2005).
16. J. Stevens *et al.*, *J. Mol. Biol.* **355**, 1143 (2006).
17. K. Shinya *et al.*, *Nature* **440**, 435 (2006).
18. M. Matrosovich, N. Zhou, Y. Kawaoka, R. Webster, *J. Virol.* **73**, 1146 (1999).
19. D. van Riel *et al.*, *Science* **312**, 399 (2006); published online 22 March 2006 (10.1126/science.1125548).
20. A. H. Reid, T. G. Fanning, J. V. Hultin, J. K. Taubenberger, *Proc. Natl. Acad. Sci. U.S.A.* **96**, 1651 (1999).
21. E. Fodor *et al.*, *J. Virol.* **73**, 9679 (1999).
22. C. F. Basler *et al.*, *Proc. Natl. Acad. Sci. U.S.A.* **98**, 2746 (2001).
23. The 1918 viruses were handled under biosafety level 3 enhanced (BSL3) containment in accordance with guidelines of the National Institutes of Health (NIH) and the Centers for Disease Control and Prevention (CDC) (available at www.cdc.gov/flu/h2n2bsl3.htm) and in accordance with requirements of the U.S. Department of Agriculture (USDA)–CDC select agent program.
24. J. Stevens *et al.*, *Science* **312**, 404 (2006); published online 15 March 2006 (10.1126/science.1124513).
25. The use of the term "respiratory droplet transmission" throughout this report refers to transmission in the absence of direct or indirect contact and does not imply an understanding of the droplet size involved in virus spread between ferrets. The ability of each virus to undergo respiratory droplet transmission among ferrets was assessed by measuring virus titers in nasal washes from contact animals every other day for 9 days. HI analysis was also performed on postexposure ferret sera collected 18 days p.c. Although only single experiments are reported, there was little variation in the replication and transmissibility among the three inoculated and the three contact ferrets for each of the seven H1N1 viruses tested in this study.
26. Material and methods are available on *Science* Online.
27. A. Gambaryan *et al.*, *Virology* **344**, 432 (2006).
28. G. Lamblin *et al.*, *Glycoconj. J.* **18**, 661 (2001).

29. We thank C. Chesley for critical review of the manuscript and J. Beck for technical assistance. This work was partially supported by NIH grant PO1 AI058113 (to A.G.-S.), the Northeast Biodefense Center (U54 AIO57158), and the Center for Investigating Viral Immunity and Antagonism (CIVIA) (U19 AI62623). Work in the A.G.-S. and P.P. laboratories is partially supported by the W. M. Keck Foundation. P.P. is a Senior Scholar of the Ellison Medical Foundation. This work was partially supported by Agriculture Research Service, USDA, Current Research Information System project number 6612-32000-039-00D.

Supporting Online Material

www.sciencemag.org/cgi/content/full/315/5812/655/DC1
Materials and Methods
SOM Text
Figs. S1 and S2
References

12 October 2006; accepted 13 December 2006
10.1126/science.1136212

Protein Kinase C β and Prolyl Isomerase 1 Regulate Mitochondrial Effects of the Life-Span Determinant p66^{Shc}

Paolo Pinton,[1,2]* Alessandro Rimessi,[1,2]* Saverio Marchi,[1,2] Francesca Orsini,[3,4] Enrica Migliaccio,[3,4] Marco Giorgio,[3,4] Cristina Contursi,[5] Saverio Minucci,[5] Fiamma Mantovani,[6,7] Mariusz R. Wieckowski,[1,2,8] Giannino Del Sal,[6,7] Pier Giuseppe Pelicci,[3,4,9] Rosario Rizzuto[1,2]†

The 66-kilodalton isoform of the growth factor adapter Shc (p66^{Shc}) translates oxidative damage into cell death by acting as reactive oxygen species (ROS) producer within mitochondria. However, the signaling link between cellular stress and mitochondrial proapoptotic activity of p66^{Shc} was not known. We demonstrate that protein kinase C β, activated by oxidative conditions in the cell, induces phosphorylation of p66^{Shc} and triggers mitochondrial accumulation of the protein after it is recognized by the prolyl isomerase Pin1. Once imported, p66^{Shc} causes alterations of mitochondrial Ca^{2+} responses and three-dimensional structure, thus inducing apoptosis. These data identify a signaling route that activates an apoptotic inducer shortening the life span and could be a potential target of pharmacological approaches to inhibit aging.

The protein p66^{Shc} (*1–4*) is an alternatively spliced isoform of a growth factor adapter that is phosphorylated upon oxidative stress (*2*). Ablation of the p66^{Shc} gene causes life-span prolongation with no pathological consequence (*2*). A fraction of p66^{Shc} localizes to mitochondria (*3–5*), where it binds to cytochrome c and acts as oxidoreductase, generating reactive oxygen species (ROS) and leading to organelle dysfunction and cell death (*5*). The route leading to p66^{Shc} activation is still unclear. Phosphorylation of a critical serine (Ser^{36}) is necessary (*2*), but the kinase responsible has not been identified. Moreover, mitochondrial p66^{Shc} is unphosphorylated, indicating that additional regulatory elements must exist.

Mitochondria receive, under stimulation by physiological agonists or toxic agents, Ca^{2+}-mediated inputs (*6–8*) that are decoded into effects as diverse as metabolic stimulation and apoptosis (*9*). Ca^{2+} responsiveness is a highly sensitive readout of mitochondrial state: Partial defects in mitochondrial energization, as in mitochondrial diseases, cause defects in Ca^{2+} handling by the organelle (*10*). Moreover, mitochondrial Ca^{2+} uptake is modulated by regulatory proteins such as kinases. Some protein kinase C (PKC) isoforms (*11*) specifically affect the responses of mitochondrial Ca^{2+} to agonists (PKCβ reduces them, whereas PKCζ enhances them) (*12*). PKCs are also proposed to be activated in conditions of oxidative stress (*13*). We therefore used aequorin to monitor cellular concentrations of Ca^{2+}, a green fluorescent protein with mitochondrial presequence (mtGFP) to monitor organelle structure, and other molecular tools to clarify the signaling route linking the oxidative challenge to the activation of p66^{Shc} proapoptotic effect within

[1]Department of Experimental and Diagnostic Medicine, Section of General Pathology and Interdisciplinary Center for the Study of Inflammation (ICSI), University of Ferrara, Ferrera, Italy. [2]Emilia Romagna Laboratory for Genomics and Biotechnology (ER-Gentech), University of Ferrara, Ferrera, Italy. [3]Department of Experimental Oncology, European Institute of Oncology, Milan, Italy. [4]Fondazione Italiana per la Ricerca sul Cancro (FIRC) Institute of Molecular Oncology, Milan, Italy. [5]Congenia s.r.l., Milan, Italy. [6]Laboratorio Nazionale, Consorzio Interuniversitario per le Biotecnologie, Area Science Park, Trieste, Italy. [7]Department of Biochimica Biofisica Chimica delle Macromolecole, University of Trieste, Italy. [8]Department of Cellular Biochemistry, Nencki Institute of Experimental Biology, Polish Academy of Sciences, Poland. [9]Department of Medicine and Surgery, University of Milan, Italy.

*These authors contributed equally to this work.
†To whom correspondence should be addressed. E-mail: r.rizzuto@unife.it

mitochondria in mouse embryonic fibroblasts (MEFs) (*14*).

Using an aequorin probe targeted by a mitochondrial presequence (mtAEQ) (*15*), we investigated organelle Ca^{2+} responses to adenosine triphosphate (ATP), an extracellular agonist that causes the release of Ca^{2+} from the endoplasmic reticulum. $p66^{Shc-/-}$ and wild-type MEFs showed similar responses of $[Ca^{2+}]_m$ to ATP, both in amplitude and in kinetics (Fig. 1, A and B). This reflects a close similarity in the global Ca^{2+} signaling patterns. Indeed, the monitoring of concentration of free cytosolic Ca^{2+} ($[Ca^{2+}]_c$) showed that the $[Ca^{2+}]_c$ rises evoked by ATP in $p66^{Shc-/-}$ and wild-type MEFs were virtually superimposable (Fig. 1, A and B, insets).

To investigate the effect of an oxidative challenge, we treated cells for 30 min before the application of ATP with various concentrations of H_2O_2. Reduction of mitochondrial Ca^{2+} responses and fragmentation of the three-dimensional mitochondrial network (*16*) was observed in wild-type MEFs (Fig. 1, A and a) several hours before signs of apoptosis (cell shrinkage and nuclear condensation, for example) were detected (fig. S1), whereas minor changes in the Ca^{2+} response and morphology were detected in $p66^{Shc-/-}$ MEFs (Fig. 1, B and b). This alteration in Ca^{2+} response was characteristically mitochondrial, because no difference in the ATP-dependent $[Ca^{2+}]_c$ rise was detected between $p66^{Shc-/-}$ and wild-type H_2O_2-treated MEFs (Fig. 1, A and B, insets). The reintroduction of $p66^{Shc}$ reestablished sensitivity to H_2O_2 in $p66^{Shc-/-}$ MEFs (Figs. 1C-c).

Production of ROS by $p66^{Shc}$ (*5*) influences the opening of the mitochondrial permeability transition pore (PTP) (*17*). We thus investigated whether the Ca^{2+} and morphology changes triggered by H_2O_2 could be prevented by the PTP blocker cyclosporine A (CsA). In CsA-treated wild-type MEFs, the rise in $[Ca^{2+}]_m$ evoked by ATP stimulation in the presence of H_2O_2 was largely restored (Fig. 2A) and the integrity of the mitochondrial network was preserved (Fig. 2a). On the contrary, no effect of CsA on $p66^{Shc-/-}$ (Fig. 2A, inset) or on MEFs not treated with H_2O_2 (fig. S2, A and B) was detected. Similar results were obtained with bongkrekic acid, another PTP inhibitor (fig. S2, C and c). Mitochondrial Ca^{2+} responses and morphology were not modified by H_2O_2 application to $p66^{Shc-/-}$ MEFs in which either the $p66^{Shc}$E132Q-E133Q mutant ($p66^{Shc}$qq), incapable of binding cytochrome c (*5*) (Fig. 2, B and b), or the $p66^{Shc}$S36A mutant (*2*) (Fig. 2, C and c) had been reintroduced, indicating that both the oxidoreductase activity of $p66^{Shc}$ and the phosphorylation of Ser^{36} are essential for the H_2O_2-induced proapoptotic changes.

Overexpression of the PKC isoform β reduces transient changes in $[Ca^{2+}]_m$ in HeLa (*12*), and PKCβ is expressed in MEF cells (fig. S3A). After application of H_2O_2, membrane staining of GFP-tagged PKCβ was detected by fluorescence microscopy (fig. S4A), showing its activation (*13*). Phosphorylated $p66^{Shc}$ was detected after treatment of cells with H_2O_2 or with 12-*O*-tetradecanoylphorbol 13-acetate (TPA), a PKC activator (Fig. 3A) (*14*). Hispidin, a specific blocker of the PKCβ isoform (fig. S4B) (*18*), inhibited $p66^{Shc}$ phosphorylation in both conditions (Fig. 3A).

Overexpression of PKCβ mimicked the activation of the endogenous kinase by oxidative

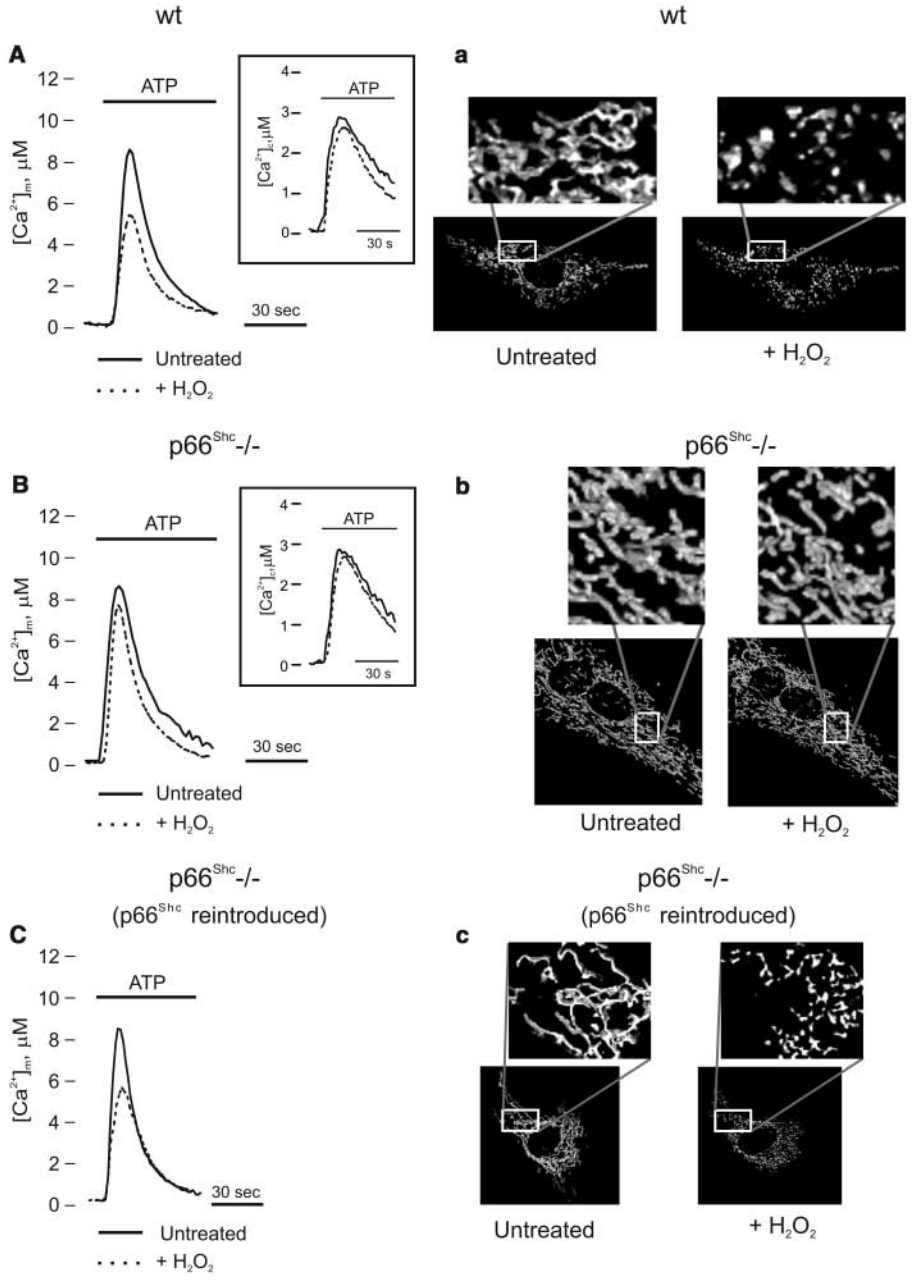

Fig. 1. Mitochondrial morphology and Ca^{2+} responses in $p66^{Shc}$ MEFs during oxidative stress. Mitochondrial and cytosolic (inset) Ca^{2+} homeostasis in wild-type (wt) (**A**) and $p66^{Shc-/-}$ (**B**) MEFs. Where indicated, mitochondrially targeted aequorin (mtAEQ)–transfected cells were treated with 100 μM ATP. wt: mitochondrial calcium concentration ($[Ca^{2+}]_m$) peak, 8.64 ± 0.32 μM; cytosolic calcium concentration ($[Ca^{2+}]_c$) peak, 2.90 ± 0.11 μM. $p66^{Shc-/-}$: $[Ca^{2+}]_m$ peak, 8.71 ± 0.37 μM; $[Ca^{2+}]_c$ peak, 2.91 ± 0.15 μM. Aequorin reconstitution and conversion of luminescence into $[Ca^{2+}]$ is described in (*14*). The dotted traces show the effect of treatment with H_2O_2 (1 mM, 30 min) on the ATP-dependent responses. wt: $[Ca^{2+}]_m$ peak, 5.84 ± 0.28 μM; $[Ca^{2+}]_c$ peak, 2.60 ± 0.07 μM. $p66^{Shc-/-}$: $[Ca^{2+}]_m$ peak, 7.87 ± 0.33 μM; $[Ca^{2+}]_c$ peak, 2.7 ± 0.09 μM. (**a** and **b**) Analysis of mitochondrial structure in cells treated with or without H_2O_2 (1 mM, 30 min) (a greater magnification is presented in the insets). (**C** and **c**) Reintroduced $p66^{Shc}$ reestablishes the $[Ca^{2+}]_m$ and morphology sensitivity to H_2O_2 in $p66^{Shc-/-}$ MEFs. $[Ca^{2+}]_m$ peak, 8.69 ± 0.51 μM; after H_2O_2, $[Ca^{2+}]_m$ peak, 5.76 ± 0.44 μM, $P < 0.01$. For all the experiments presented, $n \geq 15$.

challenges, causing a reduction in $[Ca^{2+}]_m$ responses in wild-type MEFs (in which the putative downstream effector is present) but not in $p66^{Shc-/-}$ MEFs (Fig. 3B). This effect was specific for PKCβ. When other isoforms were expressed (PKCα, PKCδ, PKCε, or PKCζ), the $p66^{Shc}$-dependent mitochondrial Ca^{2+} alteration was not observed (fig. S3). Moreover, when PKCβ was inhibited pharmacologically with hispidin (Fig. 3C) or its abundance was decreased with RNA interference (RNAi) (Fig. 3D), the $[Ca^{2+}]_m$ peak was minimally affected by the application of H_2O_2. Similarly, hispidin treatment preserved mitochondrial morphology (Fig. 3E).

We verified whether PKCβ inhibition reduced the apoptotic efficacy of H_2O_2 treatment. We measured cell viability 8 hours after the addition of 1 mM H_2O_2 by counting surviving cells on the microscopy stage. Hispidin caused no change in cell viability in wild-type cells but increased the number of cells surviving oxidative stress (29% ± 2.1 in H_2O_2-treated cells versus 60% ± 4.75 in hispidin pretreated cells, expressed as a percentage of the cells counted on a coverslip not exposed to H_2O_2) (fig. S5A).

To partially mimic an "aging" event, we analyzed mitochondrial Ca^{2+} responses in MEFs maintained in culture for 20 passages. In wild-type MEFs, the $[Ca^{2+}]_m$ responses gradually decreased with time in culture, whereas no alteration was observed in $p66^{Shc-/-}$ MEFs or in wild-type MEFs if the culture medium was supplemented with hispidin (fig. S5B). We also analyzed the effect of PKCβ on other mitochondrial parameters: mitochondrial membrane potential (ΔΨ) and production of ROS (*14*). PKCβ activation by TPA caused a gradual reduction in ΔΨ in wild-type but not in $p66^{Shc-/-}$ MEFs (Fig. 3F and fig. S5C) (*4*). An increase in ROS production was observed shortly after infection of cells with an adenoviral vector driving PKCβ expression: dihydroethidium fluorescence intensity (arbitrary units) 17.70 ± 1.2 versus 14.97 ± 1.3 in nontransduced cells, supporting the view that PKCβ triggers the oxidoreductase activity of $p66^{Shc}$.

We suspected that a possible link between PKC-dependent phosphorylation of $p66^{Shc}$ and its mitochondrial oxidoreductase activity was that phosphorylation mediated transfer of $p66^{Shc}$ from the cytosol to mitochondria. The prolyl isomerase Pin1 recognizes and induces cis-trans isomerization of pSer-Pro (or pThr-Pro) bonds, conferring phosphorylation-dependent conformational changes relevant for protein function (*19*, *20*). Moreover, $Pin1^{-/-}$ MEFs are impaired in apoptosis after exposure to ultraviolet (UVc) radiation (*21*). We identified a putative consensus for Pin1 binding (Ser^{36}/Pro^{37}) in $p66^{Shc}$. Pull-down experiments (*14*) with Pin1 linked to glutathione *S*-transferase (GST-Pin1) showed that Pin1 bound to $p66^{Shc}$ after exposure of cells to UVc radiation that caused phosphorylation of $p66^{Shc}$. This interaction appeared to be phosphorylation dependent because it was reduced by treatment of cell extracts with calf intestinal phosphatase (CIP). Furthermore, the nonphosphorylatable mutant $p66^{Shc}$S36A did not show detectable binding to Pin1 (Fig. 4A).

We investigated the mitochondrial effects of H_2O_2 treatment in $Pin1^{-/-}$ MEFs. In $Pin1^{-/-}$ cells, the H_2O_2-dependent reduction of the $[Ca^{2+}]_m$ peak was smaller than that of wild-type MEFs (Fig. 4B). Similarly, in $Pin1^{-/-}$ MEFs, morphological changes caused by H_2O_2 were

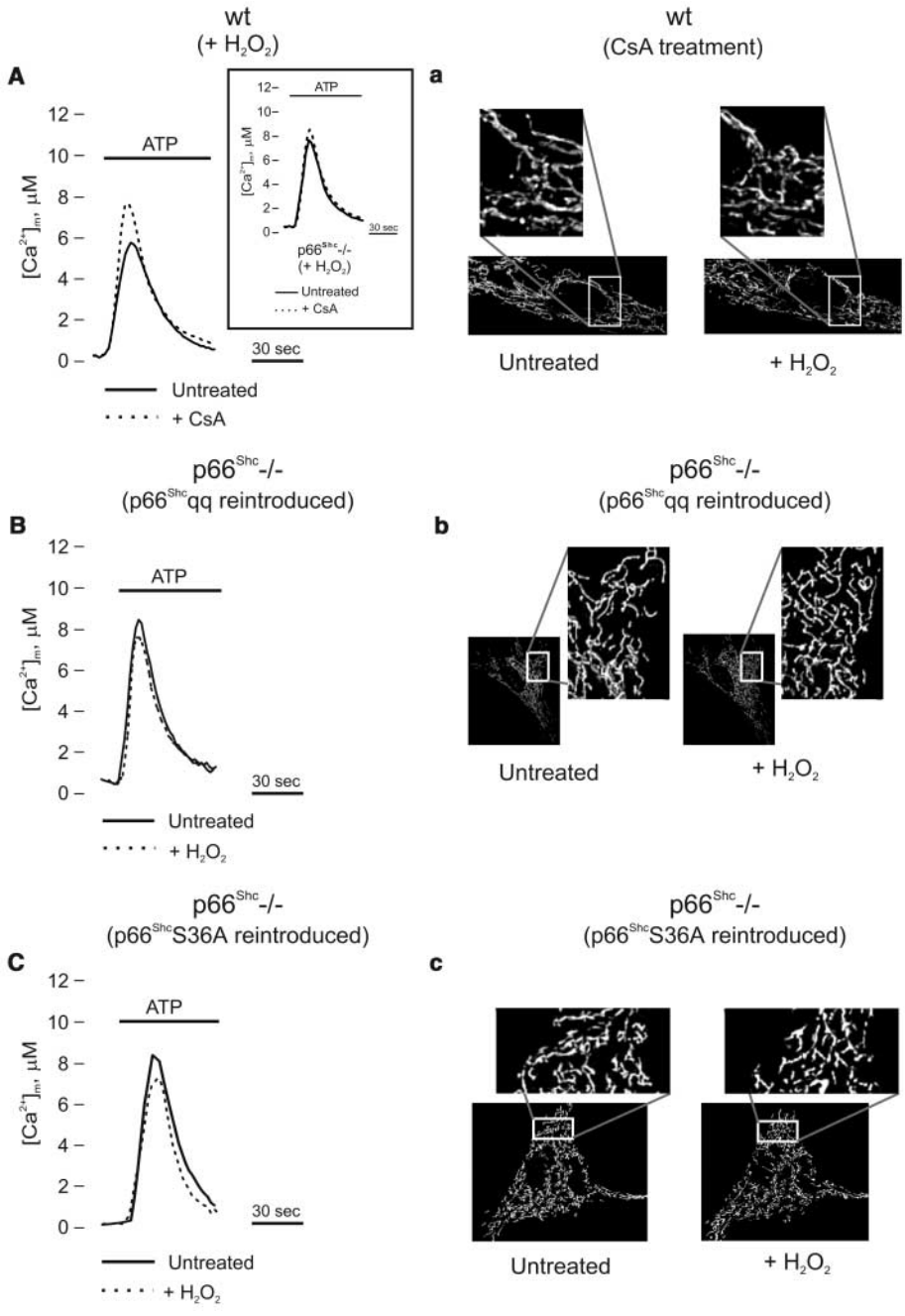

Fig. 2. Involvement of PTP, $p66^{Shc}$ binding to cytochrome c, and $p66^{Shc}$ phosphorylation in mitochondrial $p66^{Shc}$ action. (**A**) Effect of treatment with CsA (4 μM, 10 min) on H_2O_2-dependent reduction of $[Ca^{2+}]_m$ responses in wt MEFs. $[Ca^{2+}]_m$ peak, 5.84 ± 0.28 μM in cells treated only with H_2O_2; 7.58 ± 0.33 μM, $P < 0.01$, in cells pretreated with CsA, then treated with H_2O_2. No effect of CsA on $p66^{Shc-/-}$ cells was detected. $[Ca^{2+}]_m$ peak, 7.87 ± 0.33 μM in cells treated only with H_2O_2; 8.43 ± 0.54 μM in cells pretreated with CsA, then treated with H_2O_2 (Fig. 2A, inset). (**B** and **C**) Failure of the $p66^{Shc}$qq mutant ($[Ca^{2+}]_m$ peak: control, 8.35 ± 0.71 μM; H_2O_2, 7.76 ± 0.35 μM) (B) or the $p66^{Shc}$S36A mutant ($[Ca^{2+}]_m$ peak control, 8.58 ± 0.61 μM; H_2O_2, 7.74 ± 0.64 μM) (C) to reestablish mitochondrial $[Ca^{2+}]$ sensitivity to H_2O_2 in $p66^{Shc-/-}$ MEFs. All conditions as in Fig. 1. (**a** to **c**) Morphology of H_2O_2-treated, CsA-pretreated cells (a) or H_2O_2-treated cells expressing the $p66^{Shc}$qq (b) or $p66^{Shc}$S36A mutants (c).

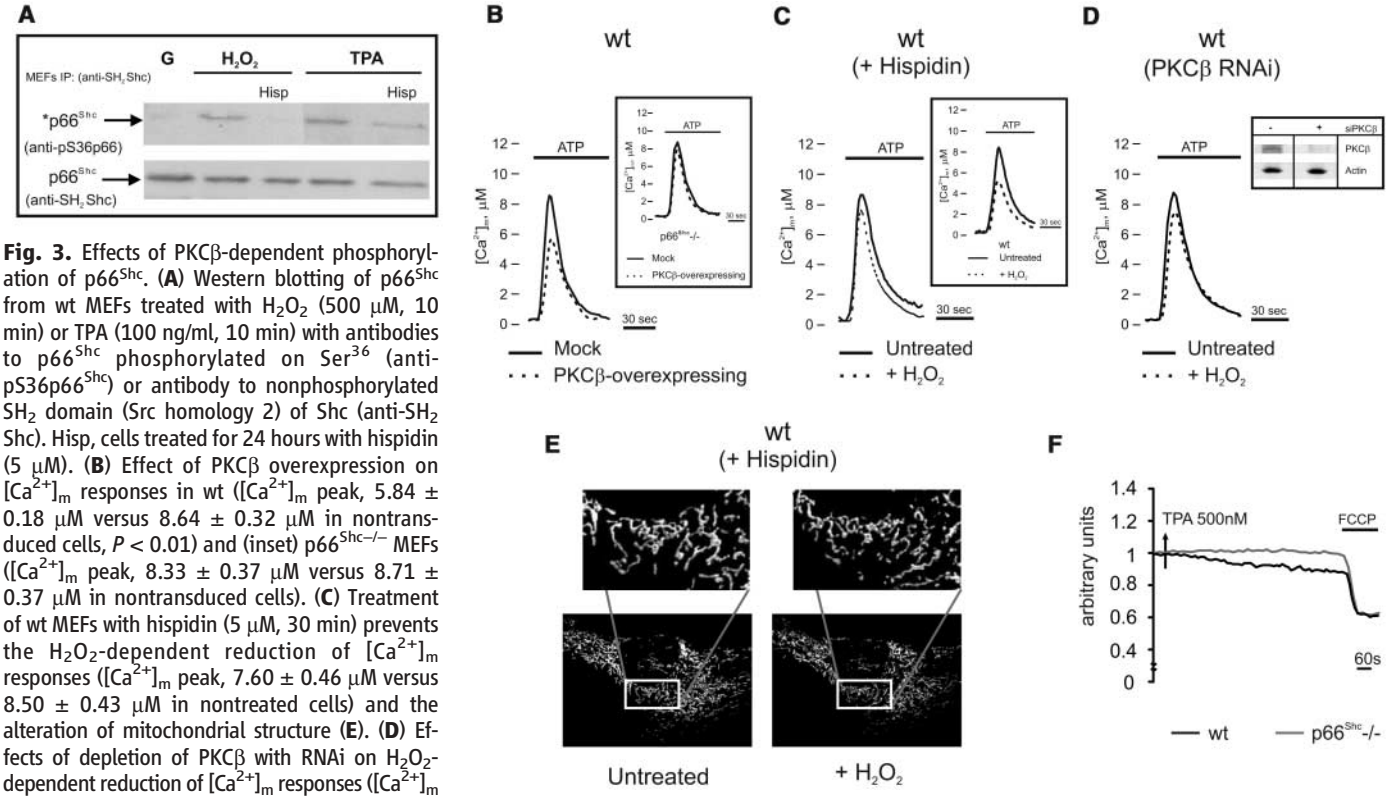

Fig. 3. Effects of PKCβ-dependent phosphorylation of $p66^{Shc}$. (**A**) Western blotting of $p66^{Shc}$ from wt MEFs treated with H_2O_2 (500 μM, 10 min) or TPA (100 ng/ml, 10 min) with antibodies to $p66^{Shc}$ phosphorylated on Ser^{36} (anti-pS36p66^{Shc}) or antibody to nonphosphorylated SH_2 domain (Src homology 2) of Shc (anti-SH_2 Shc). Hisp, cells treated for 24 hours with hispidin (5 μM). (**B**) Effect of PKCβ overexpression on $[Ca^{2+}]_m$ responses in wt ($[Ca^{2+}]_m$ peak, 5.84 ± 0.18 μM versus 8.64 ± 0.32 μM in nontransduced cells, $P < 0.01$) and (inset) $p66^{Shc-/-}$ MEFs ($[Ca^{2+}]_m$ peak, 8.33 ± 0.37 μM versus 8.71 ± 0.37 μM in nontransduced cells). (**C**) Treatment of wt MEFs with hispidin (5 μM, 30 min) prevents the H_2O_2-dependent reduction of $[Ca^{2+}]_m$ responses ($[Ca^{2+}]_m$ peak, 7.60 ± 0.46 μM versus 8.50 ± 0.43 μM in nontreated cells) and the alteration of mitochondrial structure (**E**). (**D**) Effects of depletion of PKCβ with RNAi on H_2O_2-dependent reduction of $[Ca^{2+}]_m$ responses ($[Ca^{2+}]_m$ peak, 7.43 ± 0.49 μM versus 8.81 ± 0.56 μM in nontreated cells). All conditions as in Fig. 1. Expression of PKCβ after silencing is shown in the Western blot (inset). (**F**) Kinetics of tetramethyl rhodamine methyl ester (TMRM) fluorescence of wt and $p66^{Shc-/-}$ cells treated with TPA. FCCP (carbonyl cyanide p-trifluoromethoxyphenylhydrazone), an uncoupler of oxidative phosphorylation, completely collapses the $\Delta\Psi$. The traces are representative of single cell responses.

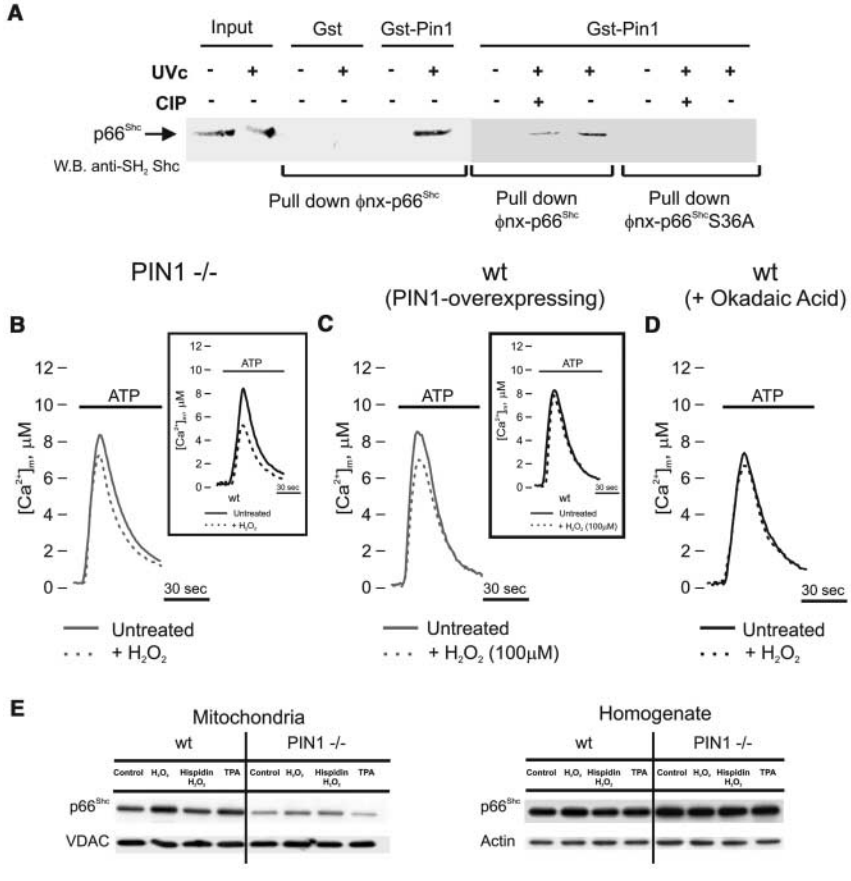

Fig. 4. Pin1 induces $p66^{Shc}$ mitochondrial translocation after Ser^{36} phosphorylation. (**A**) Total lysates from Phoenix cells (Φnx) transfected with $p66^{Shc}$ or its S36A mutant, UV-irradiated and/or treated with CIP, were subjected to GST or GST-Pin1 pull-down followed by immunoblotting with antibody to Shc. (**B**) Effect of H_2O_2 on the ATP-dependent $[Ca^{2+}]_m$ responses in $Pin1^{-/-}$ ($[Ca^{2+}]_m$ peak, 8.64 ± 0.49 μM in control versus 6.98 ± 0.46 μM in H_2O_2 treated) and (inset) wt ($[Ca^{2+}]_m$ peak, 8.41 ± 0.22 μM in control versus 5.02 ± 0.39 μM, $P < 0.01$ in H_2O_2 treated) MEFs. (**C**) Effect of 100 μM H_2O_2 on $[Ca^{2+}]_m$ responses in Pin1 overexpressing MEFs ($[Ca^{2+}]_m$ peak, 8.60 ± 0.58 μM in control versus 7.26 ± 0.26 μM H_2O_2 treated, $P < 0.05$) and (inset) in wt MEFs ($[Ca^{2+}]_m$ peak, 8.64 ± 0.49 μM in control versus 8.56 ± 0.31 μM, H_2O_2 treated). (**D**) Effects of okadaic acid (1 μM, 1 hour) on H_2O_2-dependent reduction of $[Ca^{2+}]_m$ responses ($[Ca^{2+}]_m$ peak, 7.58 ± 0.33 μM versus 6.83 ± 0.24 μM, in okadaic acid pretreated cells before and after H_2O_2 treatment, respectively). All conditions as in Fig. 1. (**E**) Western blot of $p66^{Shc}$ protein levels in the mitochondrial fraction and in the cell homogenate from wt and $Pin1^{-/-}$ MEFs.

minimal (fig. S6A). Overexpression of Pin1 sensitized cells to weaker oxidative stress. When wild-type MEFs were subjected to mild oxidative stress (100 μM H_2O_2 for 15 min instead of 1 mM for 30 min), no alteration in the agonist-dependent $[Ca^{2+}]_m$ transient was detected, whereas in Pin1 overexpressing cells, the peak was reduced (Fig. 4C). In certain substrates, the phosphoserine-proline (phosphoS-P) sites, once isomerized by Pin1, are recognized and dephosphorylated by PP2A (*20*). In cells treated with okadaic acid (PP2A inhibitor), the reduction in agonist-dependent $[Ca^{2+}]_m$ responses was markedly smaller (Fig. 4D) than that in wild-type cells, which might suggest that dephosphorylation by PP2A follows Pin1 recognition and is necessary for the mitochondrial effects of $p66^{Shc}$.

Finally, we tested the hypothesis that Pin1-dependent isomerization of $p66^{Shc}$ enhances the transfer of the protein to the organelle. We evaluated the mitochondrial pool of $p66^{Shc}$ in wild-type and $Pin1^{-/-}$ MEFs by subcellular fractionation and immunoblotting (Fig. 4E and fig. S6B) (*14*). In wild-type cells, oxidative stress increased the amount of $p66^{Shc}$ within mitochondria (~+100%). This effect appeared to depend on PKC activity, because a similar increase was evoked by treatment of cells with TPA, and hispidin inhibited the effects of H_2O_2 treatment. Blots of total homogenate showed only a small increase in the total amount of $p66^{Shc}$ (~+15%) (*4*), indicating that there was net translocation of $p66^{Shc}$ to the organelle. In $Pin1^{-/-}$ MEFs, the mitochondrial fraction of $p66^{Shc}$ was smaller, both at rest or after treatment with H_2O_2 or TPA. TPA had no detectable effect on localization of $p66^{Shc}$ in the $Pin1^{-/-}$ cells.

Overall, these data highlight a molecular route that links an oxidative challenge to the activation of $p66^{Shc}$ and the recruitment of mitochondria in apoptosis and may contribute to the aging properties of this protein.

References and Notes

1. G. M. Martin, S. N. Austad, T. E. Johnson, *Nat. Genet.* **13**, 25 (1996).
2. E. Migliaccio *et al.*, *Nature* **402**, 309 (1999).
3. S. Nemoto *et al.*, *J. Biol. Chem.* **281**, 10555 (2006).
4. F. Orsini *et al.*, *J. Biol. Chem.* **279**, 25689 (2004).
5. M. Giorgio *et al.*, *Cell* **122**, 221 (2005).
6. R. Rizzuto, P. Bernardi, T. Pozzan, *J. Physiol.* **529**, 37 (2000).
7. M. D. Bootman, P. Lipp, M. J. Berridge, *J. Cell Sci.* **114**, 2213 (2001).
8. G. Szalai, R. Krishnamurthy, G. Hajnoczky, *EMBO J.* **18**, 6349 (1999).
9. M. R. Duchen, *Cell Calcium* **28**, 339 (2000).
10. M. Brini *et al.*, *Nat. Med.* **5**, 951 (1999).
11. H. Mellor, P. J. Parker, *Biochem. J.* **332**, 281 (1998).
12. P. Pinton, S. Leo, M. R. Wieckowski, G. Di Benedetto, R. Rizzuto, *J. Cell Biol.* **165**, 223 (2004).
13. R. Gopalakrishna, S. Jaken, *Free Radic. Biol. Med.* **28**, 1349 (2000).
14. Materials and Methods are available as supporting material on *Science* Online.
15. R. Rizzuto *et al.*, *Science* **280**, 1763 (1998).
16. P. Pinton *et al.*, *EMBO J.* **20**, 2690 (2001).
17. P. Bernardi, V. Petronilli, F. Di Lisa, M. Forte, *Trends Biochem. Sci.* **26**, 112 (2001).
18. C. Gonindard *et al.*, *Cell Biol. Toxicol.* **13**, 141 (1997).
19. K. P. Lu, Y. C. Liou, X. Z. Zhou, *Trends Cell Biol.* **12**, 164 (2002).
20. G. Wulf, G. Finn, F. Suizu, K. P. Lu, *Nat. Cell Biol.* **7**, 435 (2005).
21. P. Zacchi *et al.*, *Nature* **419**, 853 (2002).

22. We thank C. Baldini for carrying out some experiments, G. A. Rutter for aequorin adenoviruses, and T. Pozzan for helpful discussion. This work was supported by grants from the Italian University Ministry (MUR), Telethon, Italy (grants GGP05284 and GTF02013), NIH (grant: A mitochondrial longevity pathway: $p66^{shc}$ mechanisms), NeuroNE, the Italian Association for Cancer Research (AIRC), the Italian Space Agency (ASI), European Union (fondi strutturali Obiettivo 2), and the Industrial Research program (PRRIITT) of the Emilia Romagna region.

Supporting Online Material

www.sciencemag.org/cgi/content/full/315/5812/659/DC1
Materials and Methods
Figs. S1 to S6
References

21 September 2006; accepted 6 December 2006
10.1126/science.1135380

Targeting of Diacylglycerol Degradation to M1 Muscarinic Receptors by β-Arrestins

Christopher D. Nelson,[1] Stephen J. Perry,[2]* Debra S. Regier,[3] Stephen M. Prescott,[3] Matthew K. Topham,[3] Robert J. Lefkowitz[2,4]†

Seven-transmembrane receptor (7TMR) signaling is transduced by second messengers such as diacylglycerol (DAG) generated in response to the heterotrimeric guanine nucleotide–binding protein G_q and is terminated by receptor desensitization and degradation of the second messengers. We show that β-arrestins coordinate both processes for the G_q-coupled M1 muscarinic receptor. β-Arrestins physically interact with diacylglycerol kinases (DGKs), enzymes that degrade DAG. Moreover, β-arrestins are essential for conversion of DAG to phosphatidic acid after agonist stimulation, and this activity requires recruitment of the β-arrestin–DGK complex to activated 7TMRs. The dual function of β-arrestins, limiting production of diacylglycerol (by receptor desensitization) while enhancing its rate of degradation, is analogous to their ability to recruit adenosine 3′,5′-monophosphate phosphodiesterases to G_s-coupled β_2-adrenergic receptors. Thus, β-arrestins can serve similar regulatory functions for disparate classes of 7TMRs through structurally dissimilar enzymes that degrade chemically distinct second messengers.

Stimulation of 7TMRs activates heterotrimeric guanine nucleotide–binding proteins (G proteins), initiating the production of second messenger molecules. For 7TMRs coupled to the G protein family member G_s, activation of adenylyl cyclase increases intracellular adenosine 3′,5′-monophosphate (cAMP) concentrations; 7TMRs that couple to $G_{q/11}$ stimulate phospholipase C and consequent hydrolysis of phosphatidylinositol 4,5-bisphosphate to produce inositol 1,4,5-trisphosphate and diacylglycerol (DAG) (*1*). Proper regulation of signal transduction requires G protein inactivation, degradation of second messengers, and silencing of activated receptors (desensitization) to return the cell to a basal state. Deactivation of G proteins is achieved through the intrinsic guanosine triphosphatase (GTPase) activity of the α subunit with subsequent reassembly of the inactive heterotrimeric complex. However, unlike the autocatalytic G proteins, most second messenger molecules require specific enzymes for metabolism to an inactive form. For DAG, regulation is particularly crucial because dysregulation leading to prolonged DAG signaling is tumorigenic (*2*, *3*).

The main pathway of DAG metabolism is phosphorylation by members of the family of diacylglycerol kinases (DGKs) (*4*). DGKs are predominantly cytoplasmic and translocate to the plasma membrane upon stimulation of many receptors, including 7TMRs. These enzymes catalyze the adenosine triphosphate (ATP)–dependent creation of phosphatidic acid (PA) through phosphorylation of the *sn*-3 position of DAG, thus negatively regulating DAG-dependent proteins such as protein kinase C (PKC). However, PA itself is a signaling molecule that influences vesicle trafficking (*5*), promotes translocation of the protein kinase Raf to the plasma membrane (*6*), and affects the activity of multiple enzymes, including type I phosphatidylinositol 5-kinases (*7*, *8*), PKCζ (*9*), and small GTPase proteins (*10*).

[1]Department of Biochemistry, Duke University Medical Center, Durham, NC 27710, USA. [2]Howard Hughes Medical Institute, Duke University Medical Center, Durham, NC 27710, USA. [3]Huntsman Cancer Institute and Department of Internal Medicine, University of Utah, Salt Lake City, UT 84112, USA. [4]Department of Medicine, Duke University Medical Center, Durham, NC 27710, USA.

*Present address: Neurocrine Biosciences Inc., 12790 El Camino Real, San Diego, CA 92130, USA.
†To whom correspondence should be addressed. E-mail: lefko001@receptor-biol.duke.edu.

Supporting online material

Materials and Methods

Cells, infections and transfection

MEFs derived from wild-type (wt) 129, $p66^{Shc}$-/- and Pin1-/- littermates were grown in Dulbecco's modified Eagle's medium (DMEM), supplemented with 10% fetal calf serum (FCS), in $75cm^2$ Falcon flasks. For aequorin measurements, the cells were seeded before transfection onto 13 mm glass coverslips and allowed to grow to 50% confluence. At this stage, the cells were infected with the adenovirus expressing the appropriate chimera, as previously described [1]. For analyzing mitochondrial structure, Pin1 overexpression and PKCβ translocation, the cells were transfected using lipofectamine (Invitrogen) or infected with an adenoviral vector driving PKCβ-GFP expression [2]. For retroviral infections, we used a PINCO vector expressing the $p66^{Shc}$ moiety of interest and GFP from an internal CMV promoter was used. MEFs derived from $p66^{Shc}$-/- mice were infected with vector alone, $p66^{Shc}$, the mutant incapable of binding cytochrome c $p66^{Shc}$qq [3] or the non-phosphorylatable mutant $p66^{Shc}$S36A as described previously [4]. The efficiency of infection (90%) was determined by FACS analysis of GFP positive cells 48 h after infection.

Aequorin measurements

The coverslip with the cells was incubated with 5 μM coelenterazine for 1-2 hours in DMEM supplemented with 1% FCS, and then transferred to the perfusion chamber. All aequorin measurements were carried out in KRB (Krebs-Ringer modified buffer: 125 mM NaCl, 5 mM KCl, 1 mM Na_3PO_4, 1 mM $MgSO_4$, 5.5 mM glucose, 20 mM HEPES, pH 7.4, 37°C) supplemented with 1mM $CaCl_2$. Agonists and other drugs were added to the same medium, as specified in figure legends. The experiments were terminated by lysing the cells with 100 μM digitonin in a hypotonic Ca^{2+}-rich solution (10 mM $CaCl_2$ in H_2O), thus discharging the remaining aequorin pool. The light signal was collected and calibrated into $[Ca^{2+}]$ values by an algorithm based on the Ca^{2+} response

curve of aequorin at physiological conditions of pH, [Mg^{2+}] and ionic strength, as previously described [5]. Representative traces are shown in the figures whereas the full dataset is included in the legends.

Microscopic analysis of mitochondrial structure and PKC translocation

Images of mitochondrial structure and PKC translocation were obtained by visualizing mtGFP [6] or PKC-GFP chimeras [2;7] using a digital imaging system based on a Zeiss Axiovert 200 fluorescence microscope equipped with a back-illuminated CCD camera (Roper Scientific, USA), excitation and emission filterwheels (Sutter Instrument Company, USA) and piezoelectric motoring of the z stage (Physik Instrumente, GmbH & Co., Germany). The data were acquired and processed using the MetaMorph analysis program (Universal Imaging Corporation, USA). For computational deblurring, a stack of images through the z plane was acquired (200 ms/image; 20 plans 0.5 μm apart) and processed using the EPR software developed by the Biomedical Imaging Group of the University of Massachusetts Medical School (Worcester, MA, USA) [8].

Immunoprecipitation and Western blotting

MEFs maintained in growth conditions (10% FCS) after a 24 hours pre-incubation with 5 μM hispidin (where indicated) were challenged for 10 min with 500 μM H_2O_2 or 100 ng/ml TPA. Cellular extracts were lysed in JS buffer (20 mM Tris-HCl ph 7.8, 50 mM NAF, 50 mM NaCl, 30 mM $Na_4P_2O_7$, 5 mM Sodium Orthovanadate, 1% Triton X-100) containing protease inhibitors (PMSF, leupeptin and aprotinin), immunoprecipitated with polyclonal anti-Shc antibodies (Tansduction Laboratories), and analyzed by immunoblotting with a specific monoclonal anti-phospho-(Ser36) $p66^{Shc}$ antibodies (Alexis) or with anti-Shc antibodies (Tansduction Laboratories).

Measurements of $\Delta\Psi_m$ and ROS production

$\Delta\Psi_m$ was measured using 10 nM TMRM on a confocal microscope (model LSM 510; Carl Zeiss MicroImaging, Inc.). The signal was collected as total emission >570 nm.

ROS production was measured with Dihydroethidium (DHE, Sigma Aldrich) and fluorescence was quantitated on a Spectrofluorophotometer (Shimadzu RF-5000) with excitation and emission wavelengths of 530 and 620 nm, respectively.

In vitro binding

In *GST-pull-down* assays ΦNX cells overexpressing $p66^{Shc}$ cDNA and $p66^{Shc}$S36A mutant non irradiated or UVc-irradiated (50 J/m^2 for 10 min), were lysed in JS buffer (20 mMTris-HCl pH 7.8, 50 mM NaF, 50 mM NaCl, 30 mM $Na_4P_2O_7$, 1% Triton X-100) containing freshly added protease inhibitors (1 mM phenylmethylsulfonylfluoride, 10 μg/ml leupeptin and 5 mg/ml aprotinin). Lysates were clarified by centrifugation at 4 °C and incubated (1 mg) with 10 μl of agarose beads containing GST-Pin1 proteins or control GST for 2 hours at 4 °C. In the case of phosphatase treatment, 20 U/ml of CIP (New England Biolabs) were added to the lysates and the reaction was continued for 30 min at 30 °C. The precipitated proteins were washed five times in the same buffer and subjected to immunoblotting analysis with anti-Shc antibodies.

Isolation of mitochondria

Cells were washed twice with PBS, resuspended and homogenized in a buffer containing 250 mM sucrose, 1 mM EGTA, 50 mM Tris-HCl, 1mM DTT, protease inhibitor cocktail, pH 7.4 with 40 μg of digitonin per ml in a glass homogenizer. Homogenate was centrifuged at 1,500 x g for 5 min twice. The final supernatant was collected and centrifuged at 10,000 x g for 10 min, the mitochondrial pellets were resuspended with homogenization buffer (without digitonin) and centrifuged again at 10,000 x g for 10 min. Mitochondrial pellets were disrupted in 100μl lysis

buffer at 4°C , incubated 30 min on ice and then centrifuged at 17,000 x g for 30 min. Protein concentration in the supernatant was determined by the Bio-Rad protein estimation kit.

Statistical analysis of data

Statistical data are presented as mean ± S.E.M., significance was calculated by Student's t test, and correlation analysis was done with the SigmaPlot 5.0 software (SPSS Inc.).

Legends to Supplementary Figures.

Supplementary Fig.1 Correlation between $[Ca^{2+}]_m$ reduction and apoptotic events induced by oxidative stress. The reduction of $[Ca^{2+}]_m$ preceded the apoptotic events. Indeed**,** a significant reduction of $[Ca^{2+}]_m$ was observed after 30 minutes treatment of 1mM H_2O_2 whereas only marginal apoptotic events were detected. **(A)** Apoptosis through time after severe (1mM) and milder (100μM) oxidative stress was evaluated by counting the number of surviving cells (expressed as percentage of control cells), averaging results from at least five independent experiments. **(B)** The $p66^{Shc}$-dependent mitochondrial changes develop through time and occur well before the apoptotic phenotype. $[Ca^{2+}]_m$ responses evoked by agonist stimulation are represented as percentage of those of control cells, averaging results from at least five independent experiments.

Supplementary Fig.2 Effect of treatment with CsA (4 μM, 10 minutes) on $[Ca^{2+}]_m$ responses of wt MEFs **(A)** ($[Ca^{2+}]_m$ peak 8.93 ± 0.42 μM vs. 8.64 ± 0.32 μM in non-treated cells) and $p66^{Shc}$-/- MEFs **(B)** ($[Ca^{2+}]_m$ peak 9.48 ± 0.34 μM vs. 8.71 ± 0.37 μM in non-treated cells) **(C)** Effect of treatment of wt MEFs with bongkrekic acid (10 μM, 30 minutes) on $[Ca^{2+}]_m$ response ($[Ca^{2+}]_m$ peak 7.67 ± 0.83 μM vs. 8.64 ± 0.32 μM in non-treated cells) and **(c)** on H_2O_2-dependent reduction of $[Ca^{2+}]_m$ responses ($[Ca^{2+}]_m$ peak 5.84 ± 0.28 μM in cells treated only with H_2O_2; 7.41 ± 0.60 μM, $p<0.01$, in bongkrekic acid-pre-treated then treated with H_2O_2 cells). All conditions as in Fig. S1.

Supplementary Fig.3 (A) Western blotting of PKCα, PKCβ, PKCδ, PKCε and PKCζ protein in MEFs. **(B)** PKCε overexpression has no effect on $[Ca^{2+}]_m$ response in wt ($[Ca^{2+}]_m$ peak 8.69 ± 0.42 μM vs. 8.64 ± 0.32 μM in non-transduced cells) and inset, $p66^{Shc}$-/- ($[Ca^{2+}]_m$ peak 8.67 ± 0.54 μM vs. 8.71 ± 0.37 μM in non-transduced cells) MEFs. **(C)** PKCα overexpression reduces the $[Ca^{2+}]_m$ response in wt ($[Ca^{2+}]_m$ peak 7.19 ± 0.47 μM vs. 8.64 ± 0.32 μM in non-transduced cells) and, inset,

p66^{Shc}-/- ([Ca^{2+}]$_m$ peak 7.53 ± 0.54 μM vs. 8.71 ± 0.37 μM in non-transduced cells) MEFs. **(D)** PKCζ overexpression increases the [Ca^{2+}]$_m$ response in wt ([Ca^{2+}]$_m$ peak 10.51 ± 0.77 μM vs. 8.64 ± 0.32 μM in non-transduced cells) and, inset, p66^{Shc}-/- ([Ca^{2+}]$_m$ peak 10.06 ± 0.89 μM vs. 8.71 ± 0.37 μM in non-transduced cells) MEFs. **(E)** PKCδ overexpression increases the [Ca^{2+}]$_m$ response in wt ([Ca^{2+}]$_m$ peak 10.92 ± 0.66 μM vs. 8.64 ± 0.32 μM in non-transduced cells) and, inset, p66^{Shc}-/- ([Ca^{2+}]$_m$ peak 10.63 ± 0.87 μM vs. 8.71 ± 0.37 μM in non-transduced cells) MEFs. **(F)** Pre-treatment of PKCδ–overexpressing MEFs with rottlerin (1 μM, 150 minutes) prevents the PKCδ-dependent increase of [Ca^{2+}]$_m$ response ([Ca^{2+}]$_m$ peak 9.28 ± 0.75 μM, vs. 10.92 ± 0.66 μM in non-treated cells) but not the H_2O_2-dependent reduction of [Ca^{2+}]$_m$ responses ([Ca^{2+}]$_m$ peak 6.21 ± 0.70 μM, vs. 10.04 ± 0.39 μM in non-treated cells). In the inset the H_2O_2-dependent reduction of [Ca^{2+}]$_m$ responses in wt MEFs is presented. All conditions as in Fig. S1.

Supplementary Fig.4 (A) Fluorescence image of PKCα–GFP, PKCβ–GFP, PKCδ–GFP, PKCε–GFP and PKCζ–GFP chimera transduced into wt MEFs via an adenoviral vector [2] before and after an oxidative challenge (H_2O_2 1mM, 30 minutes). Before the oxidative challenge, the PKCα–GFP, PKCβ–GFP, PKCδ–GFP, PKCε–GFP and PKCζ–GFP chimeras showed a predominantly cytosolic distribution, as previously described in other cell types. Upon application of H_2O_2 a clear membrane staining (PKCα–GFP, PKCβ–GFP, PKCδ–GFP and PKCε–GFP) or nuclear localization (PKCζ–GFP) was detected. The graph indicates the plasma membrane or nucleus translocation of PKCs-GFP expressed as the increase in fluorescence ratio with respect to time zero (calculated as a ratio of plasma membrane/cytosol or nucleus/cytosol average fluorescence). Averaging results are representative of at least five independent experiments. **(B)** Pre-treatment of PKCs-GFP MEFs with hispidin (5 μM, 30 minutes) prevents only the H_2O_2-dependent PKCβ–GFP plasma membrane translocation.

Supplementary Fig.5 (A) Cell viability after the addition of 1 mM H_2O_2 in wt and hispidin pre-treated (5 μM, 2 hours) MEFs **(B)** Mitochondrial Ca^{2+} responses in wt and $p66^{Shc}$-/- MEFs maintained in culture. Wt cells cultured in presence of hispidin were also monitored. **(C)** Average variations of tetramethyl rhodamine methyl ester (TMRM) fluorescence of wt and $p66^{Shc}$-/- cells treated with TPA as calculated for six independent experiments.

Supplementary Fig.6 (A) Analysis of mitochondrial structure in cells treated with or without H_2O_2 (1 mM, 30 minutes) (a greater magnification is presented in the insets) in Pin1-/- MEFs **(B)** Data from densitometry of the bands of four independent experiments of the Western blot of $p66^{Shc}$ protein levels presented in Fig. 4E, captured using the KODAK 1D Image Analysis software.

Reference List

S1. E. K. Ainscow and G. A. Rutter, *Biochem.J.* 353, 175-180 (2001).

S2. P. Pinton et al., *J.Biol.Chem.* 277, 37702-37710 (2002).

S3. M. Giorgio et al., *Cell* 122, 221-233 (2005).

S4. E. Migliaccio et al., *Nature* 402, 309-313 (1999).

S5. M. Brini et al., *J.Biol.Chem.* 270, 9896-9903 (1995).

S6. R. Rizzuto et al., *Curr.Biol.* 6, 183-188 (1996).

S7. A. Chiesa et al., *Biochem.J.* 355, 1-12 (2001).

S8. R. Rizzuto, W. Carrington, R. A. Tuft, *Trends Cell Biol.* 8, 288-292 (1998).

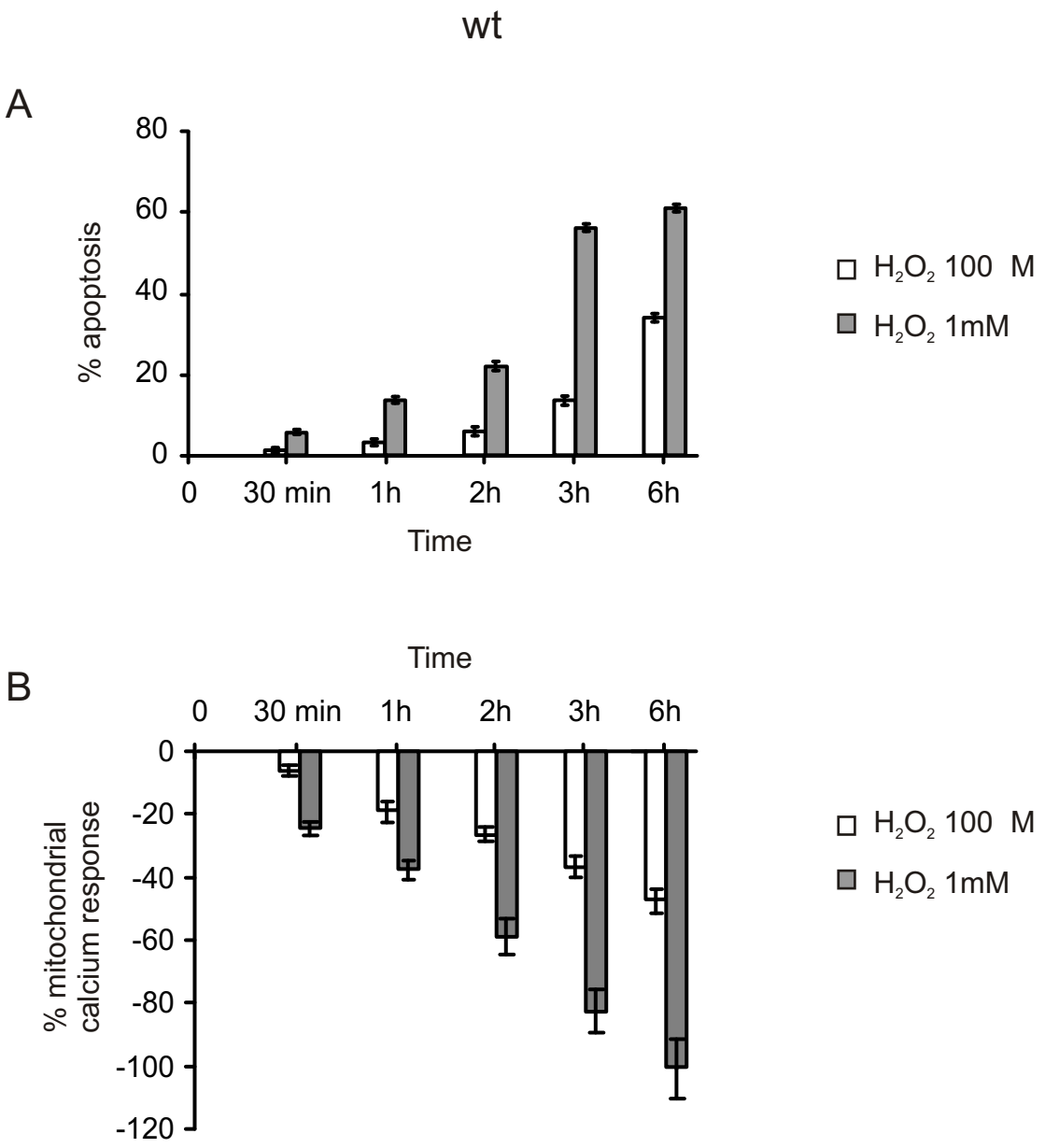

Pinton et al., Fig. S1

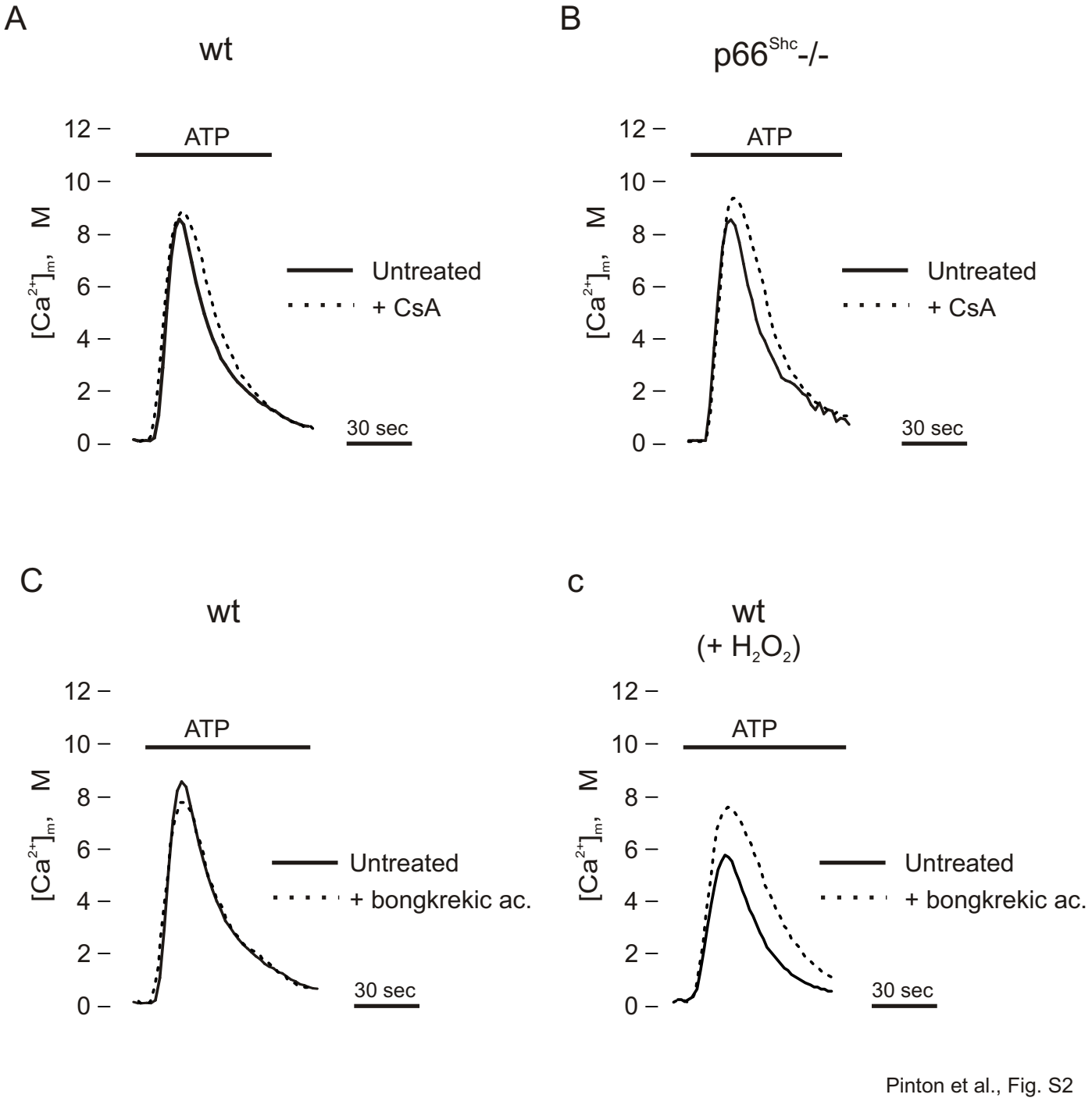

Pinton et al., Fig. S2

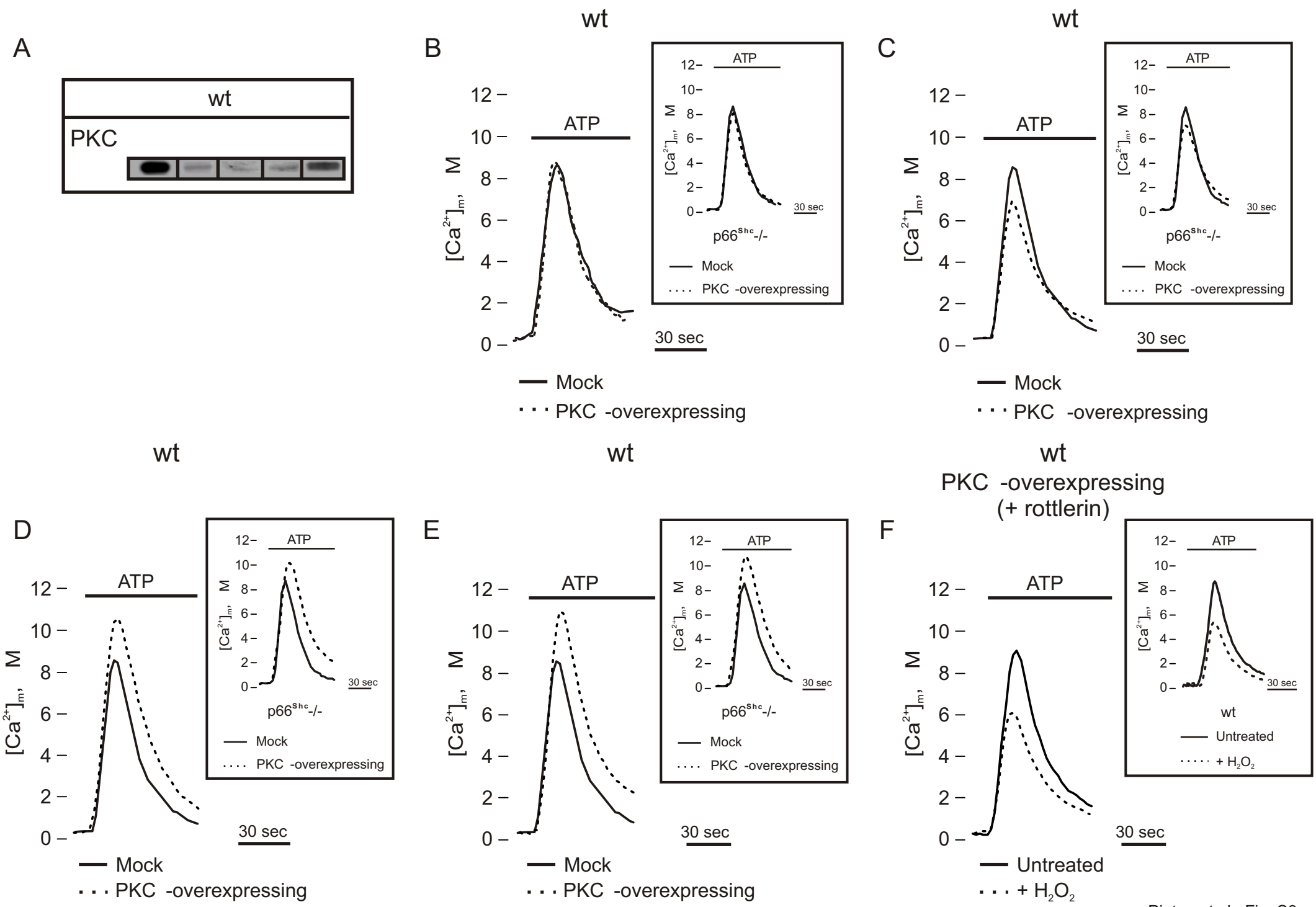

Pinton et al., Fig. S3

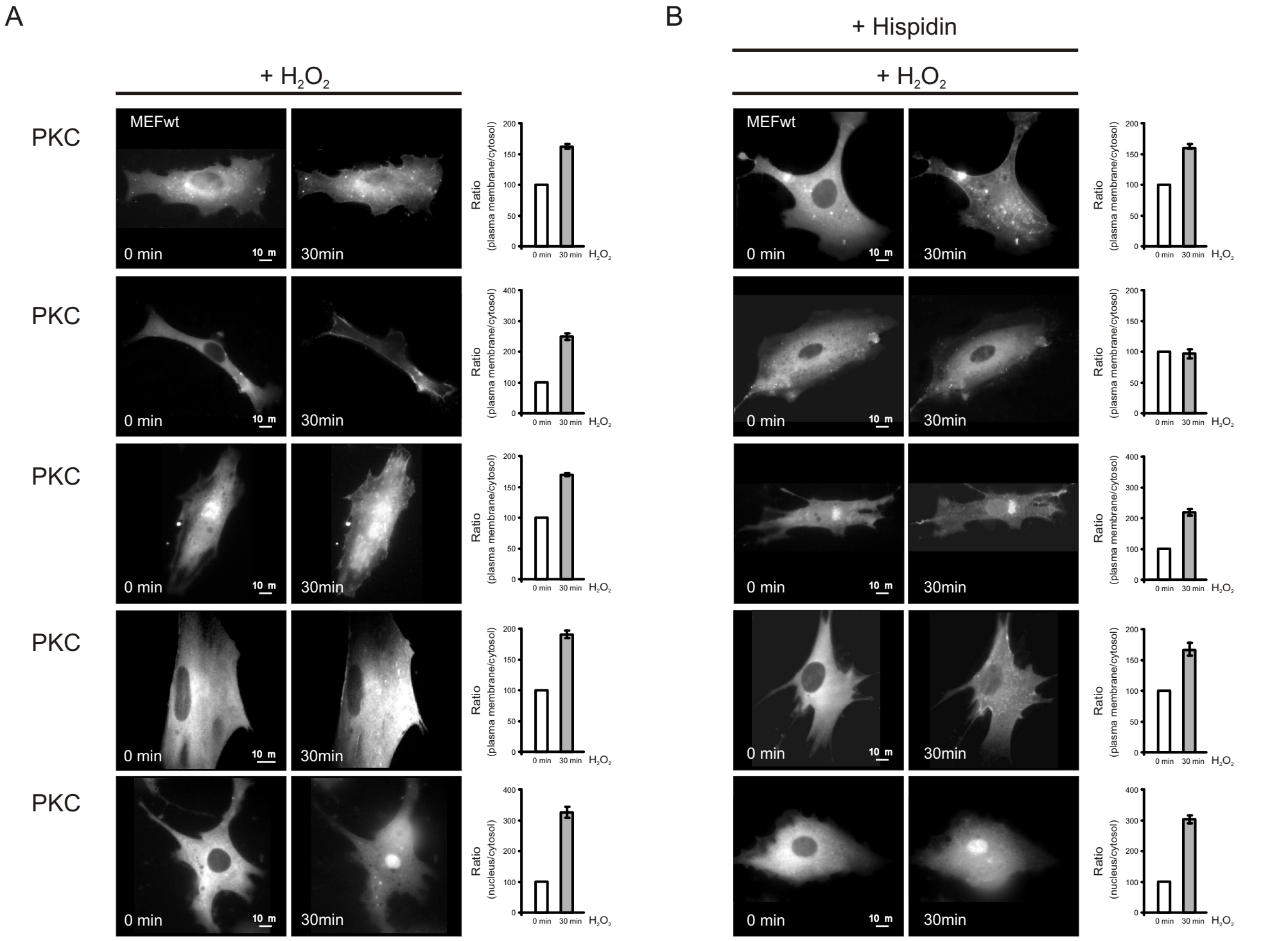

Pinton et al., Fig. S4

A

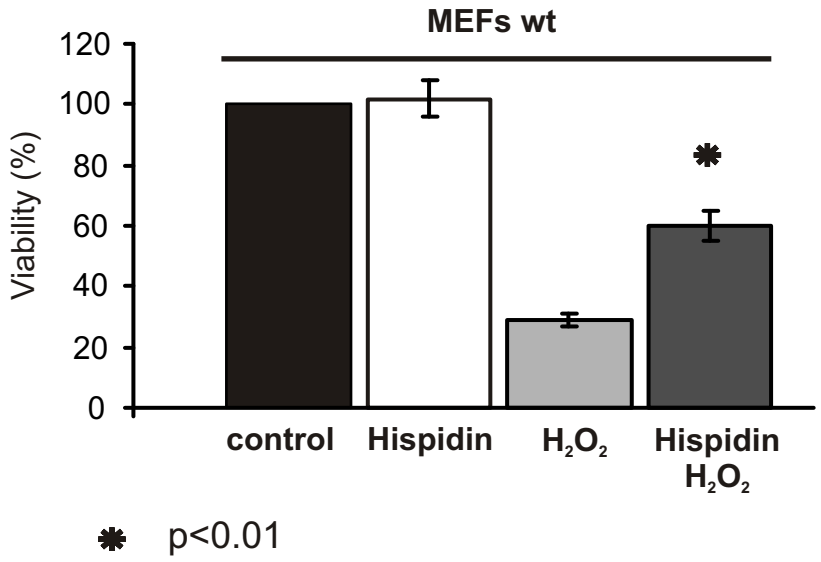

B

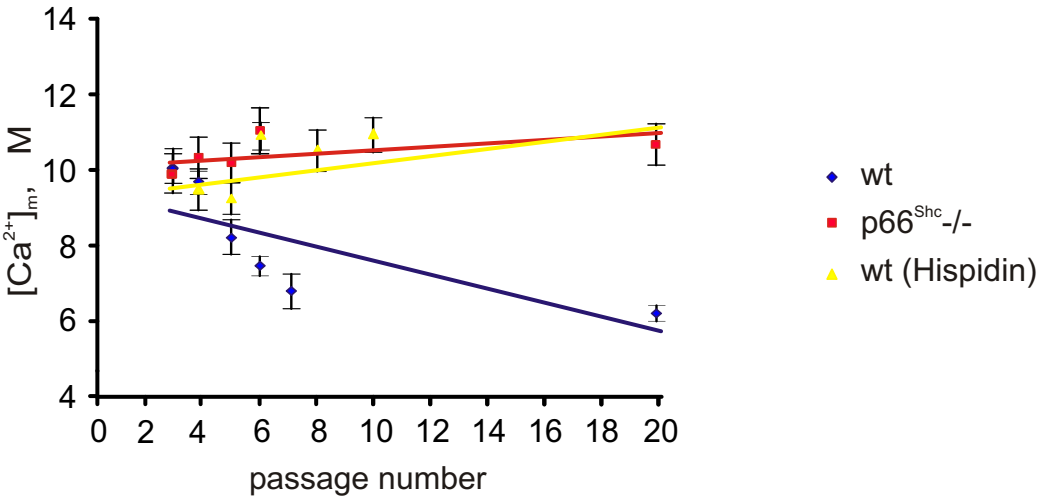

C

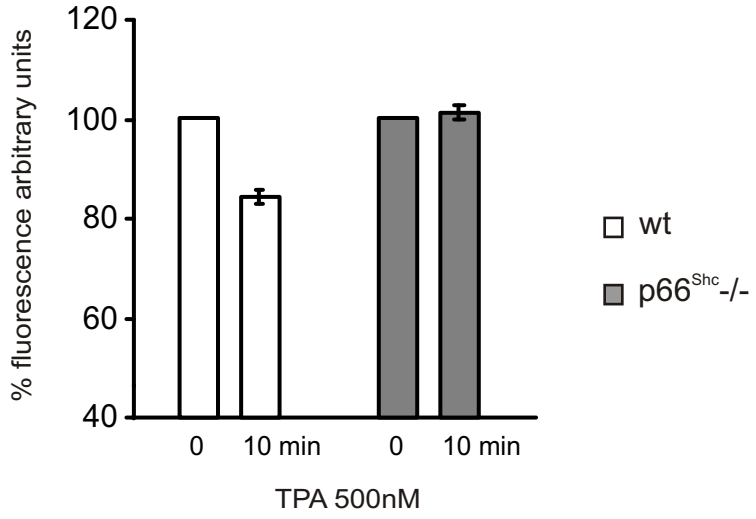

Pinton et al., Fig. S5

A

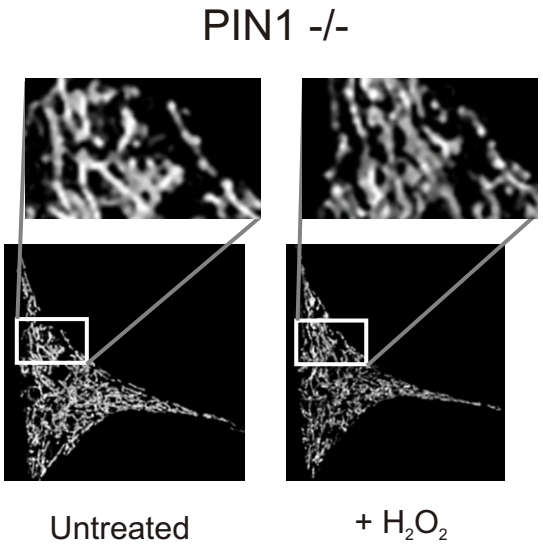

B

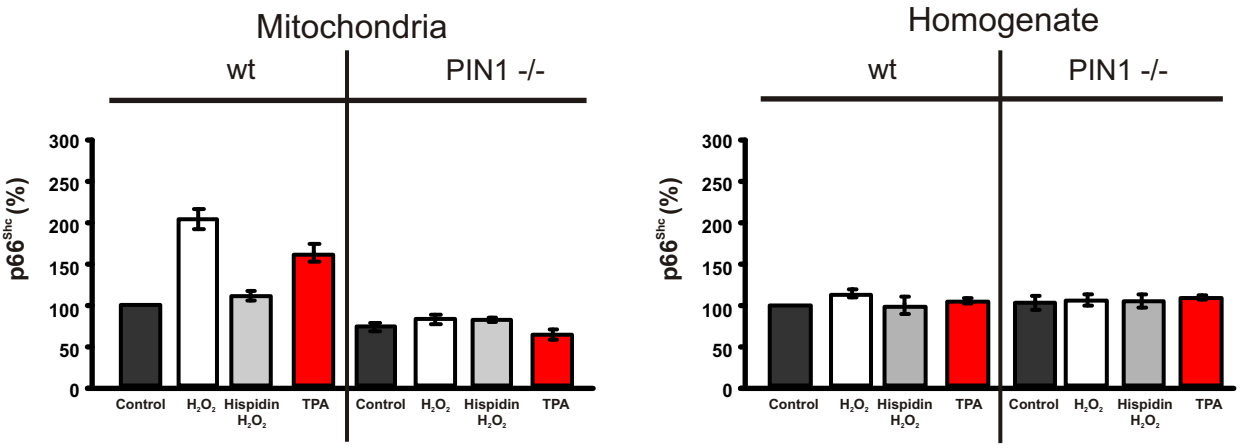

Pinton et al., Fig. S6